Global and Planetary Change 78 (2011) 178–187

Contents lists available at ScienceDirect

Global and Planetary Change

journal homepage: www.elsevier.com/locate/gloplacha

The medieval climate anomaly and the little Ice Age in coastal Syria inferred from pollen-derived palaeoclimatic patterns

D. Kaniewski [a,b,c,*], E. Van Campo [a,b], E. Paulissen [d], H. Weiss [e], J. Bakker [c,d], I. Rossignol [a,b], K. Van Lerberghe [f]

[a] Université de Toulouse, INP, UPS, EcoLab (Laboratoire Ecologie Fonctionnelle et Environnement), 118 Route de Narbonne, 31062 Toulouse, France
[b] CNRS, EcoLab, 31062 Toulouse, France
[c] Center for Archaeological Sciences, Katholieke Universiteit Leuven, Celestijnenlaan 200E, 3001 Heverlee, Belgium
[d] Physical and Regional Geography Research Group, Katholieke Universiteit Leuven, Celestijnenlaan 200E, 3001 Heverlee, Belgium
[e] Environmental Studies Program, Yale University, New Haven, CT 06520, USA
[f] Near Eastern Studies Unit, Katholieke Universiteit Leuven, Faculteit Letteren, Blijde-Inkomststraat 21, 3000 Leuven, Belgium

ARTICLE INFO

Article history:
Received 11 April 2011
Accepted 29 June 2011
Available online 19 July 2011

Keywords:
pollen-derived Biomes
numerical analyses
medieval climate anomaly
Little Ice Age
Syria

ABSTRACT

The alluvial deposits of a small spring valley near Jableh, in north-western coastal Syria, provides a unique record of environmental history covering the last 1000 years. The pollen-derived climatic proxy inferred from a 315 cm deep core of alluvial deposits suggests that a shift towards wetter climatic conditions occurred from circa (*ca.*) 1000 to 1250 calibrated (cal) yr AD. This period is situated within the time frame of the Medieval Climate Anomaly. The reconstructed temperature trends show that the warming during this medieval episode was not as high as the modern scores, except for short intervals during the early 12th century AD. The core also recorded a shift towards drier conditions starting during the late 12th century AD, which represents the Eastern Mediterranean expression of the European "Great Famine" climatic event. The main dry and cool interval recorded in coastal Syria occurred from *ca.* 1520 to 1870 cal yr AD, a time frame encompassing the Little Ice Age. In Mediterranean Syria, the Little Ice Age is not only cooler, but also much drier than the Medieval Climate Anomaly and the present-day climate. Despite a strong human presence in coastal Syria throughout the last millennia, climate rather than anthropogenic activity seems to be the driving force behind the natural vegetation dynamics in this region.

1. Introduction

The variability of the Northern Hemispheric climate during the last millennium is commonly characterized by multi-century episodes with distinct temperature and humidity anomalies: the "Medieval Climatic Anomaly/Warming" (MCA, 900–1300 AD), the "Little Ice Age" (LIA, 1300–1850 AD), and the "Modern Warming" (MW) beginning in the nineteenth century (Briffa, 2000; Verschuren et al., 2000; Briffa and Osborn, 2002; Bradley et al., 2003; Grove, 2004; Keller, 2004; Martin-Puertas et al., 2008; Helama et al., 2009; Büntgen et al., 2011. The concept of a Medieval Warm Epoch, centred on the AD 1100–1200 "High Medieval", was first articulated by Lamb (1965) for Western Europe and only concerned the positive temperature anomalies within this time frame. Since then, individual or compilation records of climate variability for the MCA in different areas over the world show both evidences for widespread temperature and hydrological anomalies from AD 900 to 1300 (Hughes and Diaz, 1994; Stine, 1994; Crowley and Lowery, 2000; Verschuren et al., 2000; Broecker, 2001; Jones et al., 2001; Bradley et al., 2003; Hunt, 2006; Osborn and Briffa, 2006; Martin-Puertas et al., 2008; Jones et al., 2009; Trouet et al., 2009). The LIA (AD 1580 to 1850) is a period of widespread temperature decline identified by synchronous negative deviations across a number of temperature-sensitive proxy records from the Northern Hemisphere (Briffa, 2000; Jacobeit et al., 2001; Jones et al., 2001; Luterbacher et al., 2004; Meyers and Pagani, 2006; Osborn and Briffa, 2006; Kuhlemann et al., 2008; Richter et al., 2009). A cold period also occurred at several locations in the Southern Hemisphere in the time frame of the LIA (Thompson et al., 1986; Pollack et al., 2006; Araneda et al., 2007).

According to model-based projections, the northern Arabian Peninsula, a crossroad between Mediterranean, continental and subtropical climates will be extremely sensitive to greenhouse warming (Alpert et al., 2008). Insights into past climate variability during historical periods in such climate hotspots are of major interest to estimate if recent climate trends are atypical or not over the last millennium. However, few palaeoenvironmental records span the MCA and LIA in the Middle East.

Alluvial deposits in Mediterranean Syria (Fig. 1) appear highly sensitive to climate shifts during the Middle-to-Late Holocene (Kaniewski

* Corresponding author at: Université de Toulouse, INP, UPS, EcoLab (Laboratoire Ecologie Fonctionnelle et Environnement), 118 Route de Narbonne, 31062 Toulouse, France. Tel.: +33 5 61 55 89 19; fax: +33 5 61 55 89 01.
E-mail address: kaniewsk@cict.fr (D. Kaniewski).

0921-8181/$ – see front matter © 2011 Elsevier B.V. All rights reserved.
doi:10.1016/j.gloplacha.2011.06.010

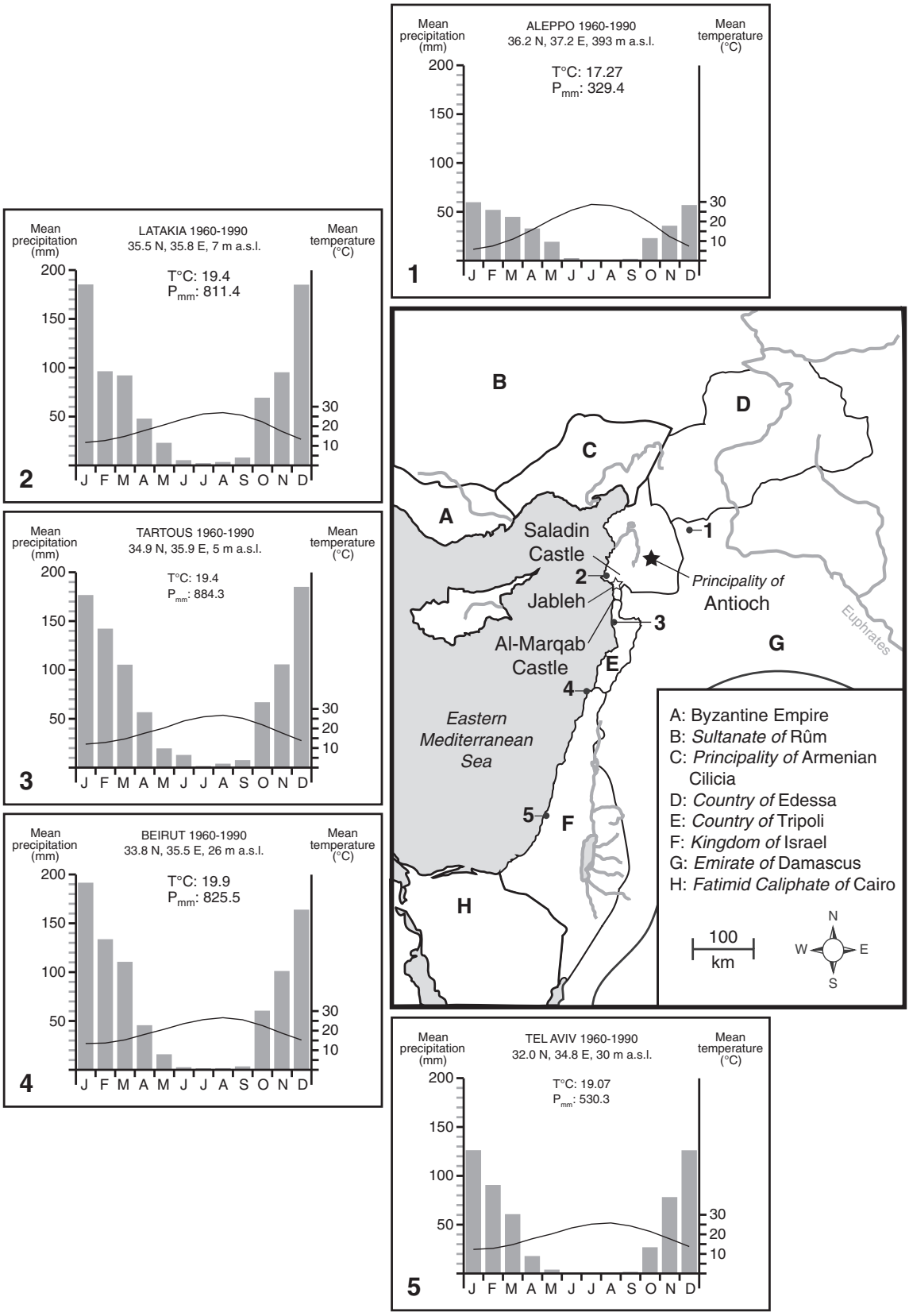

Fig. 1. Middle Ages Near Eastern Mediterranean map (12th century AD) (adapted from Muir, 1962) with overviews of the harbour town Jableh, the Saladin Castle, the Al-Marqab Castle and the borders of the Crusader states. The 1960–1990 climatograms of Aleppo, Latakia, Tartous, Beirut and Tel Aviv are depicted with the mean annual temperature (T°C) and annual precipitation amount (P_{mm}).

et al., 2008). In a first order spring valley near Jableh, thick and very recent alluvial deposits were selected to investigate the signature of climate change and human impact during the last millennium, with emphasis on the MCA and LIA. Coastal Syria is delimited towards the east by the Jabal an Nuşayrīyah, a 140 km long north-south mountain range parallel with the coast and featuring peaks above 1200 m a.s.l. During winter time, the Jabal an Nuşayrīyah range positively affects precipitation amounts in the coastal area (annual rainfall amount: 811.4 mm at Latakia; 884.3 mm at Tartous) and negatively inland (annual rainfall amount: 352.7 mm at Hama; 329.4 mm at Aleppo). Winter precipitation mainly originates from eastward propagating, mid-latitude cyclones generated in the North Atlantic and in the eastern Mediterranean Sea. During summer, the subtropical high pressure system almost completely inhibits rainfall, except during thunderstorms.

The paleoenvironmental history of coastal Syria is also of major interest due to its long human occupation. The town Jableh is situated at 28 km southwest from the 10th century AD Saladin Castle (Salah Ed-Din citadel, Soane Castle) and 25 km north from the 11th century AD Al-Marqab Castle (Kaniewski et al., 2011). Jableh was also part of the Principality of Antioch, one of the Crusader states in the Middle East (Fig. 1).

Here, we present a numerical-derived climatic proxy based on a detailed pollen record retrieved from the alluvial deposits within a 50 m broad floodplain of a spring-fed valley with a basin of about 1 km^2. The core TW-2 is situated just downstream of the confluence of the recently defunct major springs at the entrance of Tell Tweini and the Ain Fawar spring complex. This record provides the first reconstruction of the landscape dynamics in coastal Mediterranean Syria from the late 9th to the 19th centuries AD, and allows inference of climate variability within the MCA-LIA time frame.

2. Present-day vegetation

The coastal Syrian lowland, with an estimated surface of about 500 km^2, belongs to the Eu-Mediterranean biogeographical zone and is nowadays mainly under arbori-, horti- and agriculture (Fig. 2). About 25% is irrigated with waters stored in artificial lakes built in different catchments. The present-day main cultivated species are *Citrus limonum*, *Citrus sinensis*, *Nicotiana rustica*, *Prunus dulcis*, *Solanum lycopersicum*, *Zea mays* and *Olea europaea* (abandoned trees). In the study area (Fig. 2), a xeric steppe with desert scrubs and thorny-shrubs (*Artemisia herba-alba*, *Ephedra fragilis*, *Juniperus oxycedrus, Noaea mucronata*, *Prosopis stephaniana*, *Sarcopoterium spinosum*, *Zizyphus lotus)* grows in the drier rain-fed spots. Other woods/shrubs (*Tamarix*, *Pistacia atlantica*, *Crataegus azarolus*, *Styrax officinalis* and *Ceratonia siliqua*) are concentrated in the wet valley bottoms. The 650 km^2 forest area on the Jabal an Nuşayrīyah consists of oak-Juniper woodlands (*Quercus calliprinos*, *Quercus aegilops*, *Quercus infectoria*, *Juniperus excelsa*) with rare cedars (*Cedrus libani*), and degraded pine forest (*Pinus brutia* and rare *Pinus halepensis*). *Vitis vinifera* is lacking.

3. Materials and methods

3.1. Lithology and core chronology

The 315 cm core TW-2 (35°22′13.16″N, 35°56′11.36″E; 16.06 m a.s.l.) was retrieved from the recent alluvial deposits of a first order small spring-fed valley, at 1.70 km from the coast. It is an affluent valley of the River Rumailiah where Middle-to-Late Holocene alluvial deposits from this location (core TW-1) (Fig. 2) have been studied previously (Kaniewski et al., 2008).

The chronology of core TW-2 (Fig. 3) is based on three accelerator mass spectrometry (AMS) ^{14}C ages on charcoals (Table 1) at 315 cm (1170 ± 35 ^{14}C yr BP), 127 cm (875 ± 30 ^{14}C yr BP), and 94 cm (290 ± 40 ^{14}C yr BP). The 2 sigma confidences (Reimer et al., 2009) give a range of, respectively, 770–980 cal yr AD (intercept: 885 cal yr AD), 1040–1230 cal yr AD (intercept: 1168 cal yr AD), and 1480–1660 cal yr AD (intercept: 1640 cal yr AD; computed by Beta Analytic). Although any single value, neither the intercept nor any other calculation, adequately describes the complex shape of a radiocarbon probability density function (Telford et al., 2004), a single value has to be used to calculate the time-scale for numerical analyses. No gaps or unconformities were observed in the core logs and laboratory data. Compaction corrected deposition rates have been computed between the intercepts of adjacent ^{14}C ages. The values are from bottom to top: 6.65 mm yr^{-1} during 280 yr (885–1168 cal yr AD), 0.75 mm yr^{-1} during 470 yr (1168 and 1640 cal yr AD), and 2.90 mm yr^{-1} during 360 yr (1640 cal yr AD-AD 2000) (Fig. 3). Because samples have been taken at regular distances on the 315 cm sediment column, the time resolution is directly dependent on the sedimentation rate. The calculated time resolution between 2 samples is less than 10 yr (32 samples) from 885 to 1168 cal yr AD, about 70 yr (7 samples) from 1168 to 1640 cal yr AD, and about 20 yr (12 samples) from 1640 to 1870 cal yr AD. Plant remains are scarce in the core, limiting an extended chronology.

3.2. Pollen

A total of 51 samples were prepared for pollen analysis using the standard palynological procedure for clay samples described by Faegri and Iversen (1989). The prepared residues were mounted unstained in bi-distilled glycerine. Pollen grains were counted under ×400 and ×1000 magnification using an Olympus microscope. Pollen frequencies are based on the terrestrial pollen sum (average: 545 pollen grains) excluding local hygrophytes and spores of non-vascular cryptogams. Aquatic taxa frequencies are calculated by adding the local hygrophytes-hydrophytes to the terrestrial pollen sum. The aquatic taxa scores were calculated by summing the local hygrophytes-hydrophytes. The Eastern Mediterranean primary anthropogenic indicators scores (*Fraxinus ornus*, *Juglans regia*, *Vitis vinifera*, Poaceae cerealia) were calculated by summing the corresponding taxa and termed as cultivated species.

Modern pollen spectra on terrestrial surfaces are usually studied by pollen trapped by bryophytes or from soil surfaces. Due to the absence of bryophytes, superficial soil sediments were used and numbered from 1 to 12 (Fig. 2). Descriptive vegetation data were noticed for each sample location.

3.3. Numerical analyses

Pollen data have been converted into Plant Functional Types (PFTs) and a pollen-derived biomization of the PFTs has been elaborated following the appropriate methods (Prentice et al., 1996; Tarasov et al., 1998). The pollen-derived Biomes (PdBs) are similar to the regional studies in the Mediterranean and Kazakhstan (Tarasov et al., 1998), featuring Desert (DESE), Steppe (STEP), Xerophytic woods/shrubs (XERO) and Warm mixed forest (WAMX). The cultivated species are not included in the PdBs. *Olea* pollen-type has been included in the XERO PdB (Tarasov et al., 1998). The results of the numerical process used to disentangle the wild or cultivated varieties of olive tree (Kaniewski et al., 2009) suggest that *Olea europaea* is not cultivated during the Middle Ages and the Modern Era. *Olea* may result from the wild varieties (*Olea europaea* var. *sylvestris*) mixed with abandoned cultivated varieties (*Olea europaea* var. *europaea*) resulting from the Roman and Byzantine arboriculture. Olive cultivation may have been abandoned in the Jableh alluvial plain during the Muslim Era (AD 640–1095) and olive trees may have developed in coastal maquis or arborescent mattoral since then. *Olea* pollen-type in the modern samples originates from the cultivated varieties located on Tell Tweini (Fig. 2) and is only included in the cultivated species.

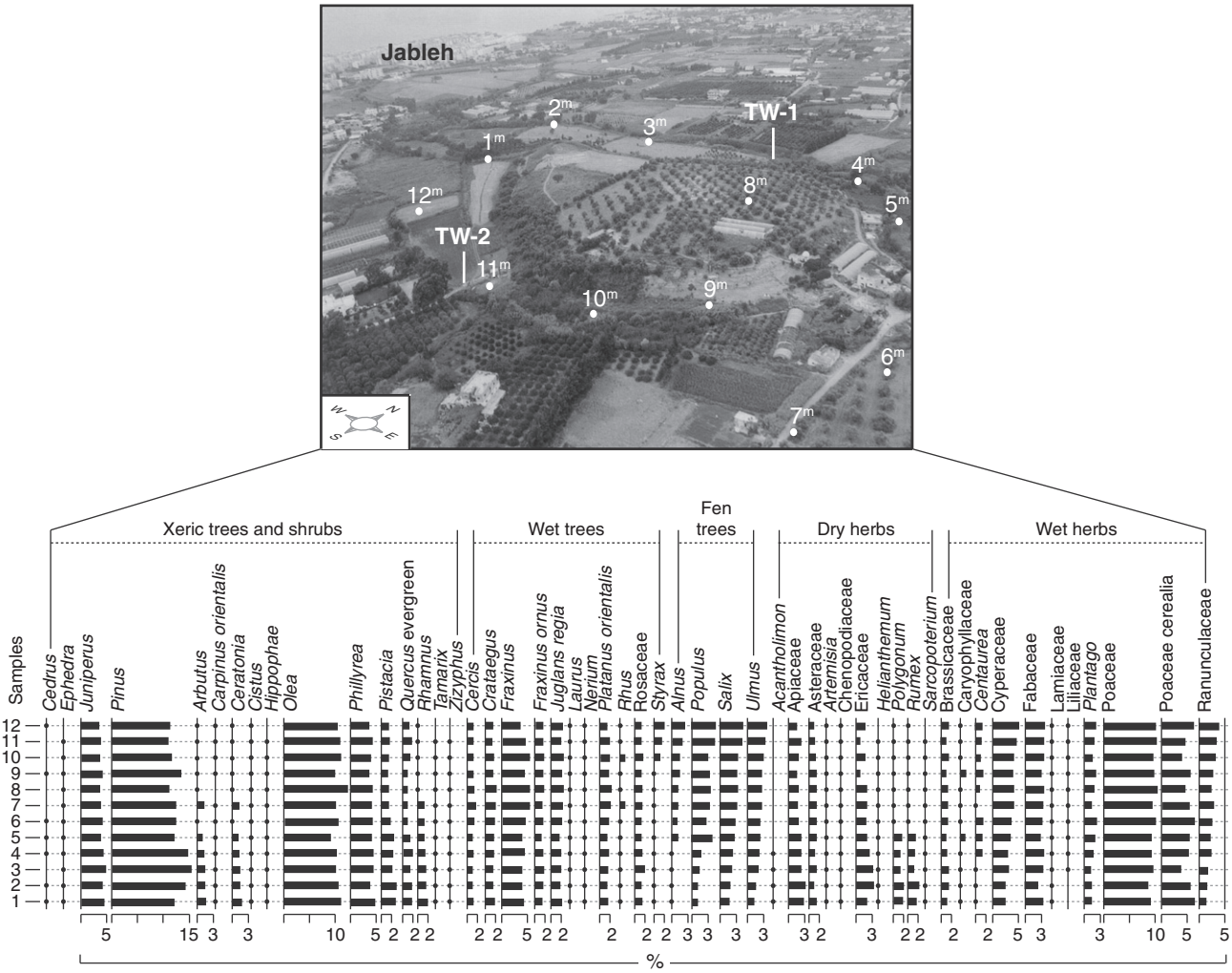

Fig. 2. Modern pollen spectra diagram and aerial photograph showing the locations of the surface samples in the alluvial plain near Jableh. The location of cores TW-1 and TW-2 is indicated.

Linear detrended cross-correlations ($P=0.05$) were applied to test the relationships between human pressure and the introduction of a steppe landscape in the Syrian coastal area (Fig. 4). Linear detrended cross-correlation concerns the time alignment of two time series by means of the correlation coefficient in a selected time-window (Kaniewski et al., 2008, 2009). The correlation coefficient is plotted

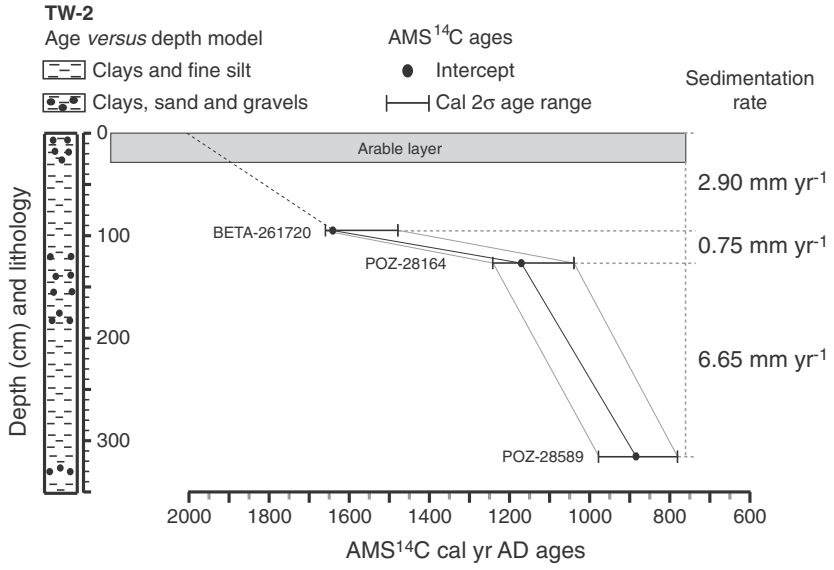

Fig. 3. AMS ^{14}C calibrated ages and suggested age-depth curves.

Table 1
Details of the ^{14}C age determinations for the TW-2 core.

Samples	Depth (cm)	Laboratory codes	Material	Conventional ^{14}C age (yr BP $\pm 1\sigma$)	cal (2σ) age range rounded (AD/BC)	cal (1σ) age range rounded (AD/BC)	Intercept (AD/BC)
TWE08 EP21	94	Beta-261720	charcoals	290 ± 40 BP	1480–1660 AD	1630–1650 AD	1640 AD
TWE08 EP27	127	Poz-28164	charcoals	875 ± 30 BP	1040–1230 AD	1150–1220 AD	1168 AD
TWE08 EP59	315	Poz-28589	charcoals	1170 ± 35 BP	770–980 AD	770–900 AD	885 AD

as a function of alignment position. This numerical approach is well-adapted to detect and quantify potential links between PdBs and the cultivated species which are direct indicators of human activities. Positive correlation coefficients are considered, focussing on the Lag 0 value (with + .50 as significant threshold). Negative correlations are also assessed to test the inverse or non-correlation between the two time-series (with −.50 as significant threshold). Null values indicate a complete lack of correlation. Human-induced changes of PdBs classified as steppe and desert (Fig. 4) may be reflected by a significant positive correlation coefficient at Lag0 ($P = 0.05$).

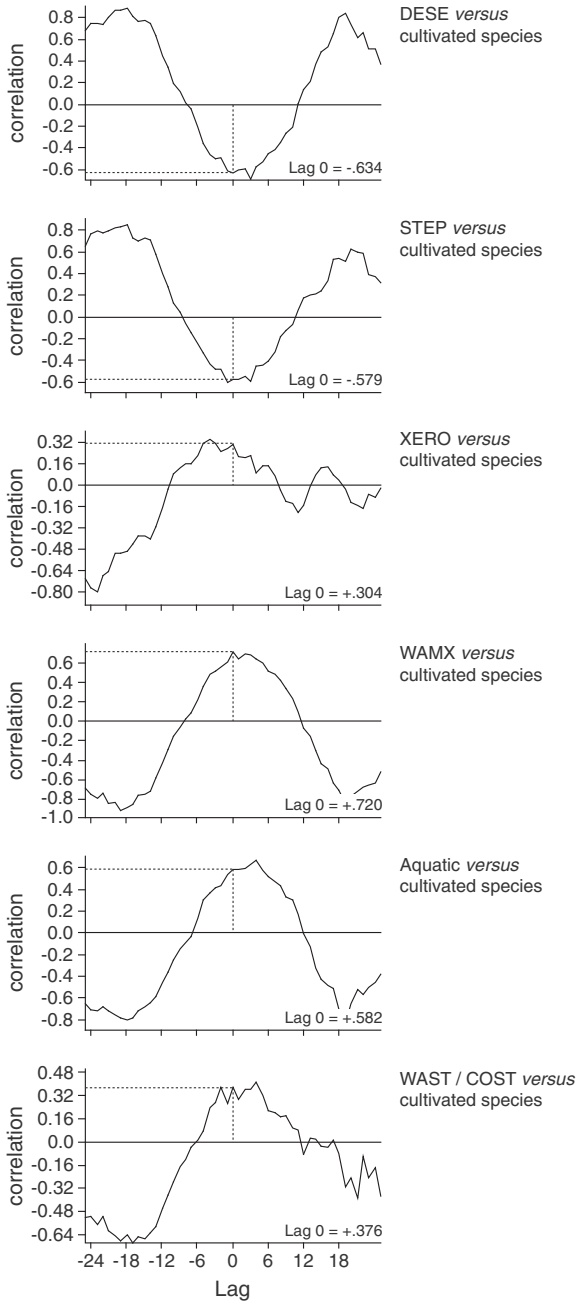

Fig. 4. TW-2 cross-correlograms: Cultivated species versus DESE, STEP, XERO, WAMX, aquatic taxa, and WAST/COST ratio. Vertical axes show correlation coefficients while horizontal axes show the lag (*1 unit = 1 sample*). Significance level $P = 0.05$.

Principal components analysis (PCA) was performed to test the ordination of samples by assessing major changes in the PdB-scores (Kaniewski et al., 2008). The main variance is loaded by the PCA-Axis1. The PdBs and the PCA-Axis1 have been plotted on a linear age-scale with cultivated species and aquatic taxa scores (Fig. 5). The ratio of PdB warm steppe (WAST) divided by PdB cool steppe (COST) (Tarasov et al., 1998), and the MCA-LIA time frames have been also added (Fig. 5). A pollen-based quantification of changes in rainfall amount or changes in temperatures was not possible. The few available regional modern pollen spectra prevent any application of a pollen-based transfer function for the time being. The modern score lines drawn on the PCA-Axis1 and WAST/COST curves (Fig. 5) correspond to the values of the modern samples (Fig. 2).

PCA was also chosen to provide a two-dimensional representation of high-dimensional geometric distances between fossil and modern samples. In this study, the second PCA (computed with all the samples, not the PdBs) was based on a covariance matrix calculated from data that have been centred to the origin of the coordinate system. A biplot PCA graph was constructed to numerically link modern and historical samples according to the pollen-derived biomes, aquatic taxa and cultivated species (Fig. 6).

4. Results

Potential influence of anthropogenic activities on the PdBs and aquatic taxa was investigated by applying linear detrended cross-correlations ($P = 0.05$) on all samples. The cross-correlograms (Fig. 4) show that the cultivated species cluster is inversely correlated with DESE (−.634) and STEP (−.579), non-significantly correlated with XERO (+.304), and WAST/COST (+.376), and significantly correlated with aquatic taxa (+.582), and WAMX (+.720). No correlations between the steppe-desert PdBs and the pollen-derived signal of human activities are evidenced.

PCA ordination was applied to the TW-2 core samples (Fig. 5). The first PCA-Axis explains 84.39% of total inertia. PCA-Axes 2 and 3 account respectively for 11.44% and 2.22% of total inertia. PCA-Axis 1 loadings are negative for the PdBs DESE (−.698) and STEP (−.387) and positive for PdBs XERO (+.309) and WAMX (+.516). Two periods of negative scores of the PCA-axis1 are recorded at *ca.* 895–1000 and *ca.* 1520–1870 cal yr AD, as well as an isolated peak at *ca.* 1315 cal yr AD (Fig. 5). These two deviations are loaded by increases of DESE-STEP PdB-scores and are correlated with decreased values of cultivated species and aquatic taxa (Fig. 5). A main positive deviation at *ca.* 1000–1240 cal yr AD is loaded by PdBs classified as wood-forest. They are well correlated with strong increases of cultivated species and aquatic taxa values (Fig. 5). The WAST/COST ratio (Fig. 5) oscillates until *ca.* 1200 cal yr AD with isolated peaks centred on *ca.* 1110–1170 cal yr AD. After *ca.* 1315 cal yr AD, the ratio values decrease and stay low until *ca.* 1870 cal yr AD. The present value at AD 2000, computed according to the modern samples, is comparable to the highest MCA values.

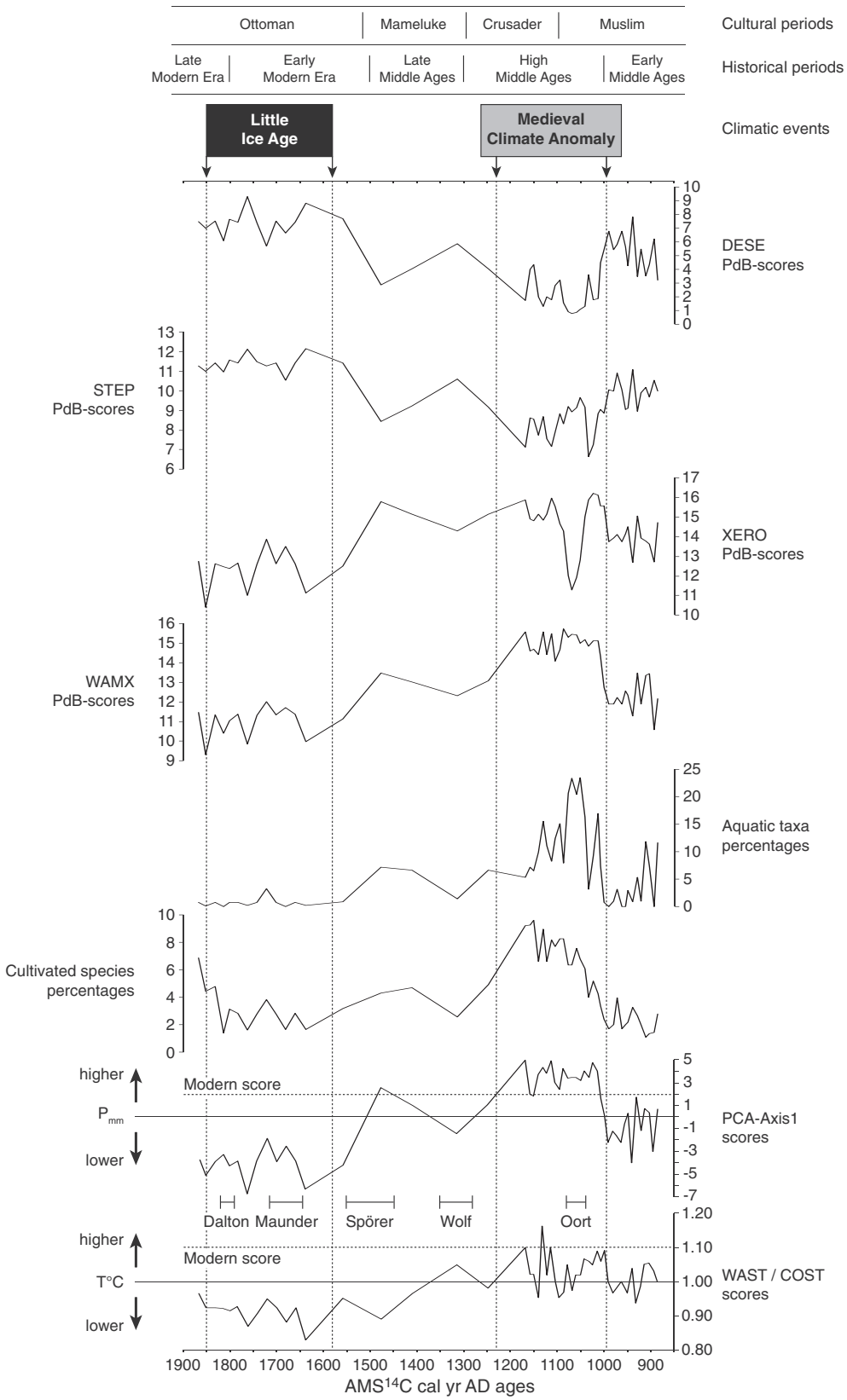

Fig. 5. The 880–1870 cal yr AD period from the viewpoint of pollen-derived climatology. The pollen-derived proxy of moisture availability is drawn as PCA-Axis 1 scores. Temperature changes are reported by the warm-cool ratio WAST/COST. The modern scores are indicated by horizontal dotted lines. The pollen-derived Biomes, the cultivated species and the aquatic taxa are shown on a linear age-scale. The main climatic events, and the historical-cultural periods are indicated at the top of the diagram. The solar minima (Oort, Wolf, Spörer, Maunder, Dalton) are underlined in grey.

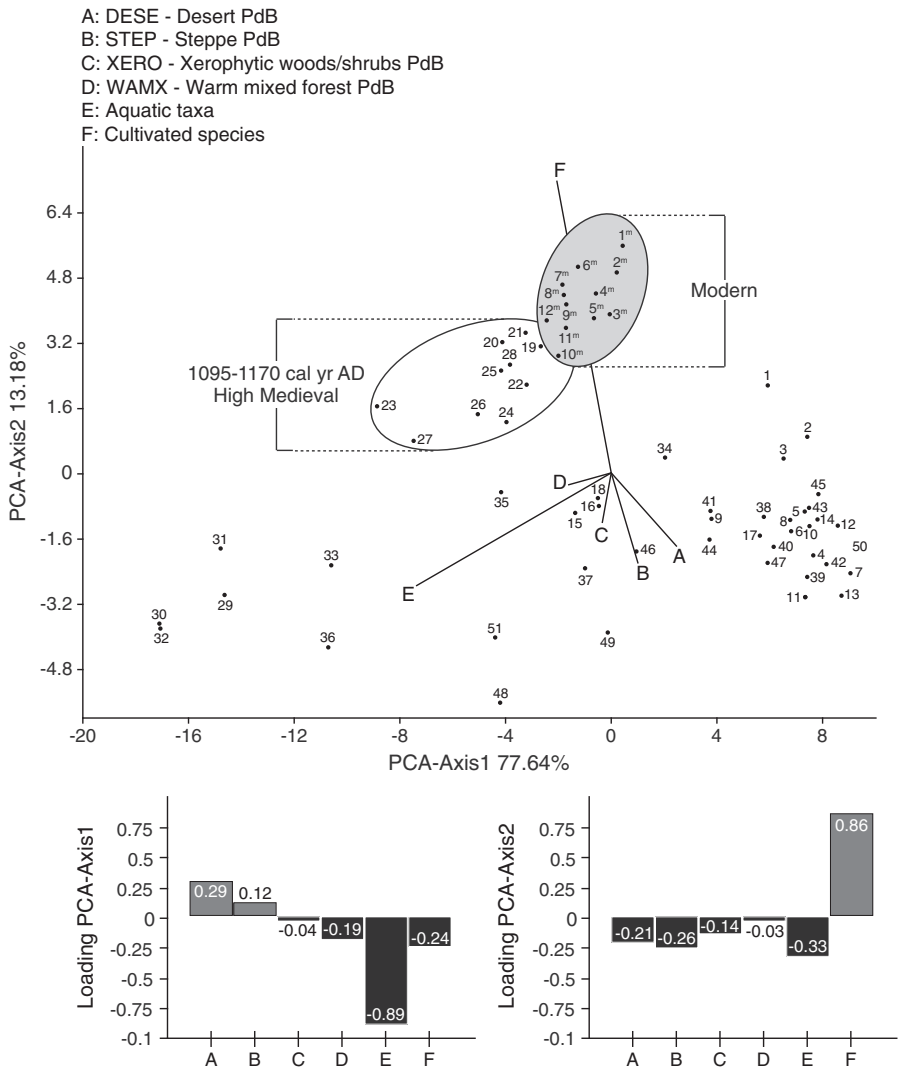

Fig. 6. - PCA biplot including modern and historical samples. PCA axes 1 and 2 account for 90.8% of the cumulative variance.

The second PCA graph (Fig. 6) (not based on PdBs) shows the ordinations of the modern and historical samples on the first and second principal components. The PCA-Axes 1 and 2 explains respectively 77.64% and 13.18% of total inertia. The 12 modern samples (AD 2000) are numerically close to the historical samples dated from *ca.* 1095 to 1170 cal yr AD.

5. Discussion

5.1. Pollen-derived climatic proxy

The lack of positive correlation between the steppe-desert PdBs, which may include secondary anthropogenic indicators (Bottema and Woldring, 1990), and the pollen-derived signal of human activities (Fig. 4), suggests no direct relationships between human pressure and the development of a steppe-landscape in the Syrian coastal area since *ca.* 885 cal yr AD. The succession of vegetation assemblages revealed by the PCA-Axis 1 ordination of the TW-2 PdB data was therefore mainly controlled by variations in moisture availability (Fig. 5). Moisture availability may come directly from rainwater in the coastal area, but also from the springs. Temperature changes (Fig. 5) are approached by the warm-cool WAST/COST ratio (Tarasov et al., 1998).

The cultivated species, the aquatic taxa (both not included in the PdBs) and the WAMX wood-forest PdB show the same dynamics, suggesting a similar response to positive shifts in humidity. Columelle (2002), a writer of the first century AD, mentioned the need of making plantations of wet trees (e.g. *Alnus*, *Populus*, and *Ulmus*) to support vine ranks. Some fen trees included in the WAMX PdB, and correlated with the cultivated species, may have been planted during wetter phases for the use of wood in the vineyard. This hypothesis cannot be excluded. *Vitis vinifera* is only strongly cultivated during the High Middle Ages in coastal Syria. This tree disappeared from the pollen sequence since *ca.* 1250 cal yr AD.

5.2. Early and High Medieval (AD 885–1300)

The *ca.* 885–1000 cal yr AD period corresponds with the development of relatively dry conditions in coastal Syria, peaking at *ca.* 945 cal yr AD (Fig. 5). This period coincides with the Muslim Era (AD 640–1095). The $\delta^{18}O$ records from Soreq Cave (Bar-Matthews et al., 2003), Ashdod coast (Schilman et al., 2001, 2002), and När Gölü (Jones et al., 2006) show higher values, indicating a similar shift toward drier conditions during this time frame as $\delta^{18}O$ high/low values correspond to low/high amounts of rainfall (Bar-Matthews et al., 2003). The northern Dead Sea basin level sharply drops to low values since 600 cal yr AD, until *ca.* 950–1000 cal yr AD Bookman (Ken-Tor) et al. (2004); Migowski et al., 2006). The Aral Sea pollen-derived climatic proxy (Sorrel et al., 2007) shows a last peak of humidity at *ca.* 750–775 cal yr AD before a dry period peaking at *ca.* 950 cal yr AD. Comparison of the hydroclimatic anomalies in Syria

with southwest Asian or northeast African tropical records shows that the fluvial inputs in the Arabian Sea off Pakistan (Von Rad et al., 1999; Lückge et al., 2001), and the Nile runoffs (Jiang et al., 2002), both correlated with precipitation amounts, decrease respectively since *ca.* 850 cal yr AD (lowest value at *ca.* 950 cal yr AD) and *ca.* 930 cal yr AD (lowest value at *ca.* 1000 cal yr AD). A weak Indian monsoon phase is also recorded before *ca.* 1000 cal yr AD (Gupta et al., 2005).

From *ca.* 1000 AD to 1250 cal yr AD, a period corresponding roughly with the Crusader period (AD 1095–1291), humid conditions prevail, whereas the WAST/COST temperature proxy does not change significantly (Fig. 5). The increasing moisture coincides with a first major increase of the cultivated species and aquatic taxa in the TW-2 core. Humid conditions also develop in southern Levant as reported by the δ^{18}O records from Soreq Cave (Bar-Matthews et al., 2003) and Ashdod coast (Schilman et al., 2001, 2002), both showing minimal δ^{18}O values between *ca.* 1050 and 1350 cal yr AD (termed Event II; Schilman et al., 2002). Increases of winter precipitation amounts are suggested at När Gölü (Jones et al., 2006). The Red Sea δ^{18}O curve (Lamy et al., 2006) shows low values suggesting wetter conditions whereas Central Asia (Sorrel et al., 2007) remains dry until *ca.* 1175 cal yr AD. Enhanced Nile floods (Hassan, 2007), higher fluvial inputs in the Arabian Sea off Pakistan (Von Rad et al., 1999; Lückge et al., 2001), stronger Indian monsoon (Gupta et al., 2005) and high water levels documented for Saharan Lakes (Nicholson, 1980) confirm similar responses in the nearby tropical zones. These evidences show that wetter climatic conditions prevailed throughout the Middle East during the time period coinciding with the known MCA (Hughes and Diaz, 1994; Stine, 1994; Crowley and Lowery, 2000; Broecker, 2001; Jones et al., 2001; Bradley et al., 2003; Hunt, 2006; Osborn and Briffa, 2006; Trouet et al., 2009). The scores of the WAST/COST temperature proxy oscillate around the 1 value, with only three high positive peaks at *ca.* 1115, 1130, and 1170 cal yr AD and three main negative deviations at *ca.* 1085–1095, *ca.* 1145, and *ca.* 1240–1260 cal yr AD (Fig. 5). The *ca.* 1240–1260 cal yr AD negative deviation may be correlated with a cold event that occurred in AD 1232. This event was characterized by the freezing of the Bosphorus (Yavuz, 2007).

5.3. Late Medieval (AD 1300–1550)

The Late Medieval, which corresponds to the Mameluke Sultanate (AD 1291–1517), appears as an unstable climatic phase characterized by an overall decrease of both moisture and temperature indicators, with a warm/dry peak at *ca.* 1315 cal yr AD. A drier phase is also evidenced by a peak of δ^{18}O values in the Ashdod coast record (Schilman et al., 2001, 2002), slight drop of the northern Dead Sea basin level Bookman (Ken-Tor) et al. (2004); Migowski et al., 2006), increased δ^{18}O values at När Gölü (Jones et al., 2006) and decrease of precipitation in Central Asia (Sorrel et al., 2007). Decrease of Nile floods (Hassan, 2007), and lower fluvial inputs in the Arabian Sea off Pakistan (Von Rad et al., 1999; Lückge et al., 2001) are also recorded. The *ca.* 1315 cal yr AD dry/warm peak chronologically coincides with the Great Famine (AD 1315–1317/1322), one of the large-scale crises that struck Europe during the early 14th century AD (Jordan, 1996). At the same time, western European climate was undergoing a slight change with cooler and wetter summers and earlier autumn storms (Lamb, 1995). The *ca.* 1400–1520 cal yr AD cool and humid pulse (Fig. 5) co-occurs with low δ^{18}O values in Ashdod coast record, peaking at *ca.* 1450 cal yr AD (Schilman et al., 2001, 2002). In Egypt, the Nile floods strongly increase since *ca.* 1350 cal yr AD and remain high until *ca.* 1500 cal yr AD (Hassan, 2007). The Red Sea δ^{18}O record also suggests wetter conditions from *ca.* 1400 to 1550 cal yr AD (Lamy et al., 2006). In Central Asia, the humid phase lasts until *ca.* 1450 cal yr AD (Sorrel et al., 2007). Extremely wet years are recorded in the north Aegean between 1341 and 1503 cal yr AD (Griggs et al., 2007). The WAST/COST minimum at *ca.* 1450–1530 cal yr AD (Fig. 5) encompasses a period of harsh winters in Turkey, with the freezing of the harbour of Istanbul in AD 1520 (Yavuz, 2007).

5.4. Little Ice Age and Modern Era (AD 1500–1870)

Dry conditions are registered after *ca.* 1500 cal yr AD until *ca.* 1870 cal yr AD, during the Ottoman Empire (AD 1517–1917), with lowest values of the PCA-Axis1 scores at *ca.* 1640, and *ca.* 1765 cal yr AD. Lowest WAST/COST scores are also recorded, with temperature minima at *ca.* 1640, *ca.* 1685, and *ca.* 1765 cal yr AD (Fig. 5). This *ca.* 270 years cold/dry interval recorded in coastal Syria coincides with the LIA climatic event (Briffa, 2000; Jones et al., 2001; Osborn and Briffa, 2006; Richter et al., 2009), a well-defined cold period, which witnessed 15 extremely harsh winters between AD 1768 an 1802 in Europe. In Crete, a mass of reports and letters mentioning drought, cold winters, great heat and out-of-season rainfall indicate severe climatic conditions between AD 1548 and 1648 (Grove, 2001). Harsh cold episodes were recorded in Crete and Greece during the winters of AD 1682/1683 (Grove, 2001) and AD 1686–1687 with the freezing of the Lake Ioannina Xoplakli et al. (2001). These events are correlated with one of the lowest points in the WAST/COST score at *ca.* 1685 cal yr AD (Fig. 5). The Bosphorus was frozen in AD 1669, 1823, 1849, 1857 and 1862 (Yavuz, 2007). A dry LIA is also evidenced by strong increases of δ^{18}O values at Ashdod coast (Schilman et al., 2001, 2002), Soreq Cave (Bar-Matthews et al., 2003), and När Gölü (Jones et al., 2006). Decreased precipitation in Central Asia (Sorrel et al., 2007), weaker Indian monsoon (Gupta et al., 2005), reduced Nile Floods (Hassan, 2007), and extreme dry events in the north Aegean (Griggs et al., 2007) are also recorded.

In Turkey, the most severe winter since the LIA occurred in AD 1928. The Golden Horn was partially frozen and ice masses from the Black Sea accumulated in the Bosphorus (Yavuz, 2007). Since AD 1930, regional temperatures increased. The modern WAST/COST score (Fig. 5), dated as AD 2000, is higher than the average MCA value except for isolated peaks at *ca.* 1115, 1130, and 1170 cal yr AD. The modern PCA-Axis1 score suggests that the *ca.* 1000–1250 cal yr AD period was wetter than the present-day in coastal Syria. The numerical distribution of samples (Fig. 6) also suggests that the closest equivalent of the modern vegetation occurred during the *ca.* 1095–1170 cal yr AD interval, a period included in the High Medieval and the MCA.

5.5. Climate

Our record indicates that temperature changes in coastal Syria are coherent with the widely documented warming during the MCA, and cooling during the LIA (Jones et al., 1998; Briffa and Osborn, 2002; Massé et al., 2008; Trouet et al., 2009). Comparison with the hydroclimatic pattern shows warm/dry conditions between *ca.* 900 and 1000 cal yr AD during the Early Middle Age, whereas High Middle Ages (AD 1000–1200) appear as a warm but much wetter interval, propitious to agricultural development. Cold/dry conditions are registered between *ca.* 1575 and *ca.* 1850 cal yr AD, during the LIA. The modern warming appears exceptional in the context of the past 1250 yr, since only three warm peaks of similar amplitude are registered during the High Middle Ages. Although further research will provide a better spatial assessment of historical climate changes in the Eastern Mediterranean, the main Syrian dry events are coherent with various other eastern Mediterranean records. The main dry events are also in phase with low Nile floods and dry episodes reported in southwest Asia, as was observed for the widespread droughts around 5200 and 4200 cal yr BP (Staubwasser and Weiss, 2006).

Several forcing mechanisms have been invoked to explain the decadal to centennial climate variability of the Eastern Mediterranean, including volcanic forcing (Stothers, 1999), solar irradiance (Versteegh, 2005) and internal climate dynamics such as North Atlantic Oscillation

(NAO) phase shifts (Cullen et al., 2002). They are not mutually exclusive and may interact to explain the complex spatial and temporal structure of the MCA and LIA periods (Shindell et al., 2003; Swingedouw et al., 2011). The control exerted by the NAO on the storm tracks affecting the Mediterranean is stronger in the western and northern Mediterranean regions (Trigo et al., 2004). A millennium-long tree-ring based drought reconstruction in Morocco shows that Mediterranean dry/wet patterns were clearly associated with positive/negative modes of the NAO (Esper et al., 2007; Trouet et al., 2009). Comparison of the Moroccan, Spanish (Martin-Puertas et al., 2008), and Syrian records suggests that the MCA/LIA century-scale changes in the hydroclimatic conditions varied oppositely in the western and eastern parts of the basin. Potentially regionalized Mediterranean rainfall patterns can be elucidated by examining relationships between these patterns and large-scale atmospheric dynamics on interdecadal timescales. They show that the winter pattern accounting for the largest part of the rainfall variance represents an west-east oscillating system with prevailing opposite pressure (mainly at upper levels) and surface conditions, referred as the Mediterranean Oscillation (MO) (Dunkeloh and Jacobeit, 2003). A strong correlation between this winter pattern and the NAO (Dunkeloh and Jacobeit, 2003) suggests a connection between the MO and the hemispheric modes of the NAO. Dominating positive modes of this circulation-precipitation winter pattern would have dominated during the MCA, in contrast to more frequent negative modes during the LIA.

6. Conclusions

The pollen-derived climatic proxy inferred from the TW-2 core is well correlated with independent proxies from the Eastern Mediterranean, Central Asia and southwestern Asia, suggesting that pollen data can be used to construct secure proxy for the palaeoclimate reconstruction of the MCA and LIA. The TW-2 core also suggests that the MCA is warmer and wetter than the LIA and slightly cooler but still wetter than the present-day. Only three peaks centred on *ca.* 1115, 1130 and 1170 cal yr AD suggest similar or warmer temperatures compared to AD 2000.

Acknowledgements

This research is funded by het Fonds voor Wetenschappelijk Onderzoek, het Onderzoeksfonds Katholieke Universiteit Leuven, the Inter-university Attraction Poles Programme VI/34, Belgian Science Policy, Belgium, by the Paul Sabatier-Toulouse3 University, and by the INSU-CNRS Paleo2-Medoriant program. The authors wish to thank the Editor, Professor Paolo A. Pirazzoli, and the two reviewers, Professor José L. Carrión and Professor Chris O. Hunt, for their critical remarks and useful recommendations.

References

Alpert, P., Krichak, S.O., Shafir, H., Haim, D., Osetinsky, I., 2008. Climatic trends to extremes employing regional modeling and statistical interpretation over the E. Mediterranean. Global and Planetary Change 63, 163–170.
Araneda, A., Torrejón, F., Aguayo, M., Torres, L., Cruces, F., Cisternas, M., Urrutia, R., 2007. Historical records of San Rafael glacier advances (North Patagonian Icefield): another clue to "Little Ice Age" timing in southern Chile? The Holocene 17, 987–998.
Bar-Matthews, M., Ayalon, A., Gilmour, M., Matthews, A., Hawkesworth, C.J., 2003. Sea-land oxygen isotopic relationships from planktonic foraminifera and speleothems in the Eastern Mediterranean region and their implication for paleorainfall during interglacial intervals. Geochimica et Cosmochimica Acta 67, 3181–3199.
Bookman (Ken-Tor), R., Enzel, Y., Agnon, A., Stein, M., 2004. Late Holocene lake levels of the Dead Sea. Geological Society of America Bulletin 116, 555–571.
Bottema, S., Woldring, H., 1990. Anthropogenic indicators in the pollen record of the Eastern Mediterranean. In: Bottema, S., Entjes-Nieborg, G., Van Zeist, W. (Eds.), Man's role in the shaping of the Eastern Mediterranean landscape. Balkema, Rotterdam, pp. 231–264.
Bradley, R.S., Hughes, M.K., Diaz, H.F., 2003. Climate in medieval time. Science 302, 404–405.
Briffa, K.R., 2000. Annual climate variability in the Holocene: interpreting the message of ancient trees. Quaternary Science Reviews 19, 87–105.
Briffa, K.R., Osborn, T.J., 2002. Blowing hot and cold. Science 295, 2227–2228.
Broecker, W., 2001. Was the Medieval warm period global? Science 291, 1496–1498.
Büntgen, U., Tegel, W., Nicolussi, K., McCormick, M., Frank, D., Trouet, V., Kaplan, J.O., Herzig, F., Heussner, K.U., Wanner, H., Luterbacher, J., Esper, E., 2011. 2500 Years of European Climate Variability and Human Susceptibility. Science 331, 578–582.
Columelle, 2002. De l'agriculture. Editions Errance, Paris.
Crowley, T.J., Lowery, T.S., 2000. How warm was the Medieval Warm Period? Ambio 29, 51–54.
Cullen, H., Kaplan, A., Arkin, P.A., deMenocal, P., 2002. Impact of the North Atlantic Oscillation on Middle Eastern climate and streamflow. Climatic Change 55, 315–338.
Esper, J., Frank, D., Büntgen, U., Vestege, A., Luterbacher, J., Xoplaki, E., 2007. Long-term drought severity variations in Morocco. Geophysical Research Letters 34. doi:10.1029/2007GL030844.
Faegri, K., Iversen, I., 1989. Textbook of pollen analysis, 4th edition. John Wiley and sons, London.
Griggs, C., DeGaetano, A., Kuniholm, P., Newton, M., 2007. A regional high-frequency reconstruction of May-June precipitation in the north Aegean from oak tree rings, A.D. 1089–1989. International Journal of Climatology 27, 1075–1089.
Grove, A.T., 2001. The Little Ice Age and its geomorphological consequences in Mediterranean Europe. Climatic Change 48, 121–136.
Grove, J.M., 2004. Little Ice Ages. Ancient and Modern, volumes 1–2, second ed. Routledge, London-New York.
Gupta, A.K., Das, M., Anderson, D.M., 2005. Solar influence on the Indian summer monsoon during the Holocene. Geophysical Research Letters 32. doi:10.1029/2005GL022685.
Hassan, F.A., 2007. Extreme Nile floods and famines in Medieval Egypt (AD 930–1500) and their climatic implications. Quaternary International 173–174, 101–112.
Helama, S., Timonen, M., Holopainen, J., Ogurtsov, M.G., Mielikäinen, K., Eronen, M., Lindholm, M., Mielikäinen, J., 2009. Summer temperature variations in Lapland during the Medieval Warm Period and the Little Ice Age relative to natural instability of thermohaline circulation on multi-decadal and multi-centennial scales. Journal of Quaternary Science 24, 450–456.
Hughes, M.K., Diaz, H.F., 1994. Was there a 'medieval warm period', and if so, where and when? Climatic Change 26, 109–142.
Hunt, B.G., 2006. The Medieval Warm Period, the Little Ice Age and simulated climatic variability. Climate Dynamics 27, 677–694.
Jacobeit, J., Jönsson, P., Bärring, L., Beck, C., Ekström, M., 2001. Zonal indices for Europe 1780–1995 and running correlations with temperature. Climatic Change 48, 219–241.
Jiang, J., Mendelssohn, R., Schwing, F., Fraedrich, K., 2002. Coherency detection of multiscale abrupt changes in historic Nile flood levels. Geophysical Research Letters 29, 112–115.
Jones, P.D., Osborn, T.J., Briffa, K.R., 2001. The evolution of climate over the last millennium. Science 292, 662–667.
Jones, M.D., Roberts, C.N., Leng, M.J., Türkeş, M., 2006. A high-resolution Late Holocene lake isotope from Turkey and links to North Atlantic and monsoon climate. Geology 34, 361–364.
Jones, P.D., Briffa, K.R., Osborn, T.J., Lough, J.M., van Ommen, T.D., et al., 2009. High-resolution palaeoclimatology of the last millennium: a review of current status and future prospects. The Holocene 19, 3–49.
Jordan, W.C., 1996. The Great Famine: Northern Europe in the Early Fourteenth Century. Princeton University Press, New Jersey.
Kaniewski, D., Paulissen, E., Van Campo, E., Al-Maqdissi, M., Bretschneider, J., Van Lerberghe, K., 2008. Middle East coastal ecosystem response to middle-to-late Holocene abrupt climate changes. Proc. Nat. Acad. Sci. USA 105, 13941–13946.
Kaniewski, D., Paulissen, E., Van Campo, E., Bakker, J., Van Lerberghe, K., Waelkens, M., 2009. Wild or cultivated Olea europaea L. in the Eastern Mediterranean during the middle-late Holocene? A pollen-numerical approach. The Holocene 19, 1039–1047.
Kaniewski, D., Van Campo, E., Paulissen, E., Weiss, H., Otto, T., Bakker, J., Rossignol, I., Van Lerberghe, K., 2011. Medieval coastal Syrian vegetation patterns in the principality of Antioch. The Holocene 21, 251–262.
Keller, C.F., 2004. 1000 years of climate change. Advances in Space Research 34, 315–322.
Kuhlemann, J., Rohling, E.J., Krumrei, I., Kubik, P., Ivy-Ochs, S., Kucera, M., 2008. Regional synthesis of Mediterranean atmospheric circulation during the Last Glacial Maximum. Science 321, 1338–1340.
Lamb, H.H., 1965. The early Medieval Warm Period and its sequel. Paleogeography, Paleoclimatology, Paleoecology 1, 13–37.
Lamb, H.H., 1995. Climate, history and the modern world. Routledge, London-New York.
Lamy, F., Arz, H.W., Bond, G.C., Bahr, A., Pätzold, J., 2006. Multicentennial-scale hydrological changes in the Black Sea and northern Red Sea during the Holocene and the Arctic/North Atlantic Oscillation. Paleoceanography 21. doi:10.1029/2005PA001184.
Lückge, A., Doose-Rolinski, H., Khan, A.A., Schulz, H., von Rad, U., 2001. Monsoonal variability in the northeastern Arabian Sea during the past 5000 years: geochemical evidence from laminated sediments. Paleogeography, Paleoclimatology, Paleoecology 167, 273–286.
Luterbacher, J., Dietrich, D., Xoplaki, E., Grosjean, M., Wanner, H., 2004. European Seasonal and Annual Temperature Variability, Trends and Extremes Since 1500. Science 303, 1499–1603.
Martin-Puertas, C., Valero-Garcés, B.L., Mata, M.P., Gonzalez-Sampériz, P., Bao, R., Moreno, A., Stefanova, V., 2008. Arid and humid phases in southern Spain during the last 4000 years: The Zonar Lake record, Cordoba. The Holocene 18, 907–921.

Massé, G., Rowland, S.J., Sicre, M.A., Jacob, J., Jansen, E., Belt, S.T., 2008. Abrupt climate changes for Iceland during the last millennium: Evidence from high resolution sea ice reconstructions. Earth and Planetary Science Letters 269, 565–569.

Meyers, S.R., Pagani, M., 2006. Quasi periodic climate teleconnections between northern and southern Europe during the 17th-20th centuries. Global and Planetary Change 54, 291–301.

Migowski, C., Stein, M., Prasad, S., Negendank, J.F.W., Agnon, A., 2006. Holocene climate variability and cultural evolution in the Near East from the Dead Sea sedimentary record. Quaternary Research 66, 421–431.

Muir, R., 1962. Muir's historical atlas, ancient, medieval and modern, 9th edition. Barnes & Noble, New York.

Nicholson, S.E., 1980. Saharan climates in historic times. In: Williams, M.A.J., Faure, H. (Eds.), The Sahara and the Nile. Balkema, Rotterdam, pp. 173–200.

Osborn, T.J., Briffa, K.R., 2006. The spatial extent of 20th-century warmth in the context of the past 1200 years. Science 311, 841–844.

Pollack, H.N., Huang, S., Smerdon, J.E., 2006. Five centuries of climate change in Australia: the view from underground. Journal of Quaternary Science 21, 701–706.

Prentice, I.C., Guiot, J., Huntley, B., Jolly, D., Cheddadi, R., 1996. Reconstructing biomes from palaeoecological data: a general method and its application to European pollen data at 0 and 6 ka. Climate Dynamics 12, 185–194.

Reimer, P.J., Baillie, M.G.L., Bard, E., Bayliss, A., Beck, J.W., et al., 2009. IntCal09 and Marine09 radiocarbon age calibration curves, 0–50,000 years cal BP. Radiocarbon 51, 1111–1150.

Richter, T.O., Peeters, F.J.C., van Weering, T.C.E., 2009. Late Holocene (0–2.4 ka BP) surface water temperature and salinity variability, Feni Drift, NE Atlantic Ocean. Quaternary Science Reviews 28, 1941–1955.

Schilman, B., Bar-Matthews, M., Almogi-Labin, A., Luz, B., 2001. Global climate instability reflected by Eastern Mediterranean marine records during the Late Holocene. Palaeogeography, Palaeoclimatology, Palaeoecology 176, 157–176.

Schilman, B., Ayalon, A., Bar-Matthews, M., Kagan, E.J., Almogi-Labin, A., 2002. Sea-Land paleoclimate correlation in the Eastern Mediterranean region during the Late Holocene. Israel Journal of Earth Sciences 51, 181–190.

Shindell, D.T., Schmidt, G.A., Miller, R.L., Mann, M.E., 2003. Volcanic and solar forcing of climate change during the preindustrial era. Journal of Climate 16, 4094–4107.

Sorrel, P., Popescu, S.M., Klotz, S., Suc, J.P., Oberhänsli, H., 2007. Climate variability in the Aral Sea basin (Central Asia) during the Late Holocene based on vegetation changes. Quaternary Research 67, 357–370.

Stine, S., 1994. Extreme and persistent drought in California and Patagonia during mediaeval time. Nature 369, 546–549.

Stothers, R.B., 1999. Volcanic dry fogs, climate cooling, and plague pandemics in Europe and the Middle East. Climatic Change 42, 713–723.

Swingedouw, D., Terray, L., Cassou, C., Voldoire, A., Salas-Mélia, D., Servonnat, J., 2011. Natural forcing of climate during the last millennium: fingerprint of solar variability. Climate Dynamics 36, 1349–1364.

Tarasov, P.E., Cheddadi, R., Guiot, J., Bottema, S., Peyron, O., Belmonte, J., Ruiz-Sanchez, V., Saadi, F., Brewer, S., 1998. A method to determine warm and cool steppe biomes from pollen data; application to the Mediterranean and Kazakhstan regions. Journal of Quaternary Science 13, 335–344.

Telford, R.J., Heegaard, E., Birks, H.J.B., 2004. The intercept is a poor estimate of a calibrated radiocarbon age. The Holocene 14, 296–298.

Thompson, L.G., Mosley-Thompson, E., Dansgaard, W., Gootes, P.M., 1986. The Little Ice Age as recorded in the stratigraphy of the tropical Quelccaya Ice Cap. Science 234, 361–364.

Trigo, R.M., Pozo-Vasquez, D., Osborn, T.J., Castro-Diez, Y., Gamis-Fortis, S., Esteban-Parra, M.J., 2004. North Atlantic Oscillation influence on precipitation, river flow and water resources in the Iberian Peninsula. International Journal of Climatology 24, 925–944.

Trouet, V., Esper, J., Graham, N.E., Baker, A., Scourse, J.D., Frank, D.C., 2009. Persistent positive North Atlantic Oscillation mode dominated the Medieval Climate Anomaly. Science 324, 78–80.

Verschuren, D., Laird, K.R., Cumming, B.F., 2000. Rainfall and drought in equatorial east Africa. Nature 403, 410–414.

Versteegh, G.J.M., 2005. Solar forcing of climate. 2: Evidence from the past. Space Science Reviews 120, 243–286.

Von Rad, U., Schaaf, M., Michels, K.H., Schulz, H., Berger, W.H., Sirocko, F., 1999. A 5000-yr record of climate change in the varved sediments from the oxygen minimum zone off Pakistan, northeastern Arabian Sea. Quaternary Research 51, 39–53.

Xoplakli, E., Maheras, P., Luterbacher, J., 2001. Variability of climate in meridional Balkans during the periods 1675–1830 and its impact on human life. Climatic Change 48, 581–615.

Yavuz, V., 2007. The frozen Bosphorus and its paleoclimatic implications based on a summary of the historical data. In: Yanko-Hombach, V., Gilbert, A.S., Panin, N., Dolukhanov, P.M. (Eds.), The Black Sea Flood Question: Changes in Coastline, Climate, and Human Settlement. Springer, Netherlands, pp. 633–649.